The Evolution of Galaxies in the FORS Deep and GOODS-S Fields

Niv Drory[1,3]
Ralf Bender[2,3]
Georg Feulner[2,3,5]
Armin Gabasch[2,3]
Ulrich Hopp[2,3]
Stefan Noll[3]
Maurilio Pannella[3]
Roberto P. Saglia[3]
Mara Salvato[3,4]

[1] University of Texas at Austin, USA
[2] Universitäts-Sternwarte München, Germany
[3] Max-Planck-Institut für Extraterrestrische Physik, Garching, Germany
[4] Caltech, Pasadena, California, USA
[5] Currently: Potsdam-Institut für Klimafolgenforschung, Germany

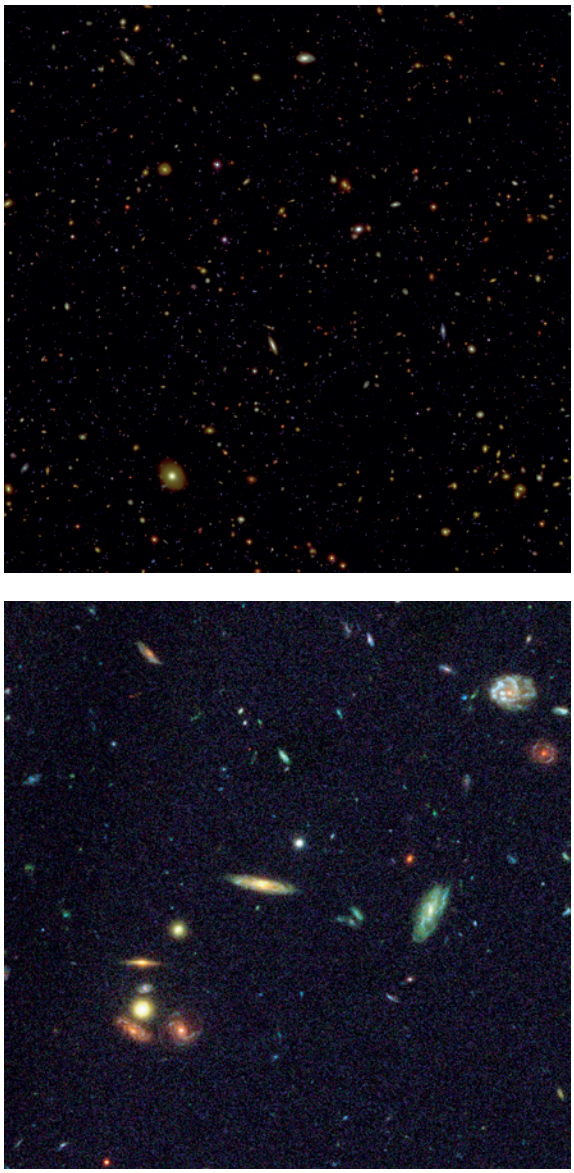

Figure 1: Composite *BRI* image of the 6 × 6 arcminute-sized FORS Deep Field (top panel) and a 1 × 1 arcminute cutout from the HST/ACS *BVz* data in the GOODS-S region (bottom panel).

Deep multicolour surveys obtained with ESO telescopes provide new insights into the evolution of galaxies from 1 Gyr after the Big Bang to the present epoch. With the broad wavelength coverage (*U* to *K*) of the FORS Deep Field and the GOODS-S field, we can derive accurate photometric redshifts for about 8000 galaxies between $z = 0$ and $z = 6$. Modelling their spectral energy distributions yields galaxy stellar masses and star-formation rates as a function of cosmic time. Interestingly, massive galaxies ($M > 10^{11}\ M_{\odot}$) seem to be present even at the highest redshift and do not disappear faster with redshift than lower-mass galaxies. Star-formation activity moves from bright to faint objects with decreasing redshift (downsizing).

The advent of 10-m-class telescopes provided the opportunity to routinely measure the evolution of galaxies as a function of redshift directly, instead of having to infer or extrapolate their evolution from information about its endpoint only, the present-day galaxy population. Large telescopes make it possible to survey huge volumes photometrically and spectroscopically to great depth and therefore obtain representative samples of galaxies spanning a large fraction of the Universe's age.

Among the parameters that have been found to evolve are stellar populations, morphology, structure, star-formation rates, and stellar and total mass. Total and stellar mass, and their change with time, are of particular importance because mass assembly is intricately linked to gravitationally driven hierarchical structure formation, which is thought to provide the wider context in which galaxy formation and evolution is to be understood. While total (baryonic and dark) mass is still very hard to measure at $z > 0$, stellar mass and star-formation rates are much more accessible to observations.

Our group is using surveys conducted with ESO facilities to study the assembly history of mass in galaxies and the history of star formation in the Universe. Results from two of these surveys having multicolour photometry and rich follow-up spectroscopy are highlighted in this article: The FORS Deep Field (FDF; Heidt et al. 2003; Noll et al. 2004) and the Great Observatories Origins Deep Survey (GOODS; Giavalisco et al. 2004) South region (for more information of the FDF see The Messenger 116, 18).

The *I*-band selected FDF photometric catalogue covering the UBgRIzJKs bands in 40 arcmin^2 is published in Heidt et al. 2003. This catalogue lists 5 557 galaxies down to $I \sim 26.8$. This sample is discussed in detail in Gabasch et al. 2004a.

Distances to all the galaxies are estimated using photometric redshift techniques, whereby the redshift is deduced by comparing each object's photometry to a library of likely galactic spectral energy distributions at various distances. These photometric redshifts for the FDF are calibrated against 362 spectroscopic redshifts up to $z \sim 5$ (Noll et al. 2004) and provide distances to an accuracy of $\Delta z/(z_{spec}+1) \leq 0.03$ with only ~ 1 % outliers (Gabasch et al. 2004a).

Our *K*-band selected catalogue for the GOODS-S/CDFS field is based on the publicly available 8 2.5 × 2.5 arcmin^2 *J*, *H*, *Ks* ISAAC images (as of version 1.1), taken at the ESO/VLT with excellent image quality (seeing in the range 0.40″–0.50″). The *U* and *I* images are from ESO GOODS/EIS public survey, while the *B*, *V*, and *R* images are taken from the Garching-Bonn Deep Survey. The catalogues are discussed and made available to the public by Salvato et al. 2006.

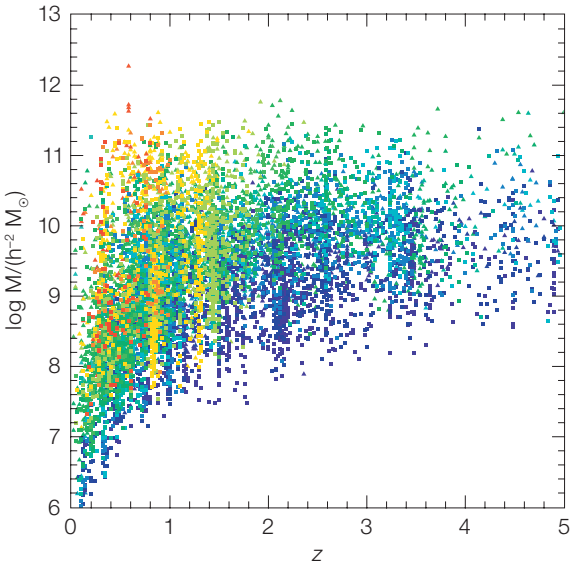

Figure 2: Stellar mass of galaxies derived from fitting stellar population models to multicolor photometry plotted against redshift (squares: FDF; triangles: GOODS). Colour encodes the effective age of the stellar population: young populations (age < 1 Gyr) are shown in blue and old population (age > 5 Gyr in red).

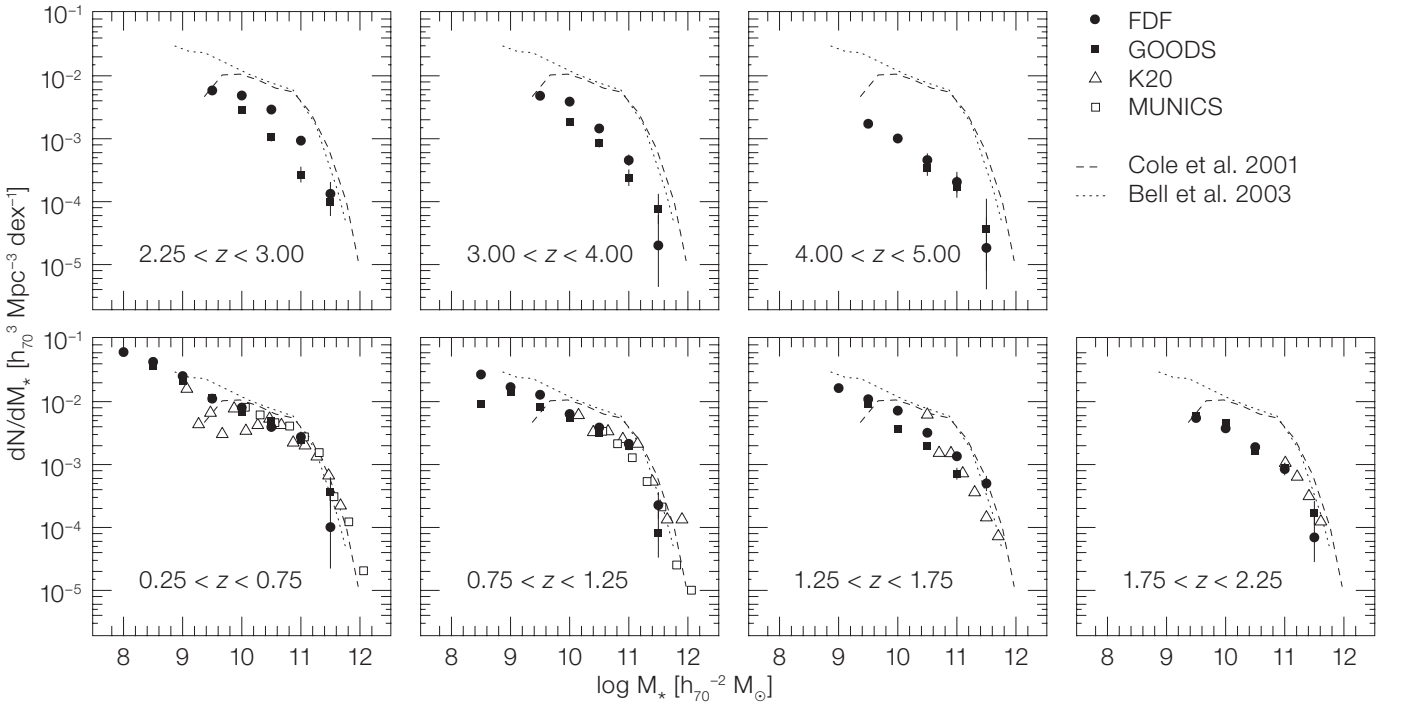

Figure 3: The stellar mass function as a function of redshift. The local mass function of is shown for comparison (dotted and dashed line). Results from the MUNICS survey (Drory et al. 2004) and the K20 survey (Fontana et al. 2004) at $z < 2$ are also shown.

In this article we will focus on the evolution of the stellar mass function (Drory et al. 2005) and the specific star-formation rates (star-formation rate per unit stellar mass; Feulner et al. 2005) of galaxies in the redshift range $0 < z < 5$. Moreover, we will study the morphological evolution up to $z \sim 1$ using HST/ACS data (Pannella et al. 2006). These observables taken together provide a valuable data set to study the mass assembly of galaxies, probing both mass and its change over time.

The stellar mass function

We derive stellar masses (the mass locked up in stars) by comparing each galaxy's multi-color photometry to a grid of stellar population synthesis models covering a wide range in parameters, such as redshift, star-formation histories, dust extinction, and starburst fractions (see Drory et al. 2004 for details).

In Figure 2 we show the distribution of galaxies in the mass versus redshift plane for the FDF (squares) and GOODS-S (triangles). In addition, we code the age of each galaxy (using the best-fitting model) in colours ranging from blue for young (age < 1 Gyr) to red for old stellar populations (age > 5 Gyr). A striking feature of Figure 2 is that the most massive galaxies harbour the oldest stellar populations at all redshifts.

Figure 3 shows the mass function (the number density of galaxies per unit log mass interval) in seven redshift bins from $z = 0.25$ to $z = 5$. For comparison, we also show the local mass function and the mass functions to $z \sim 1.2$ of MUNICS (Drory et al., 2004) and to $z \sim 2$ by the K20 survey (Fontana et al. 2004).

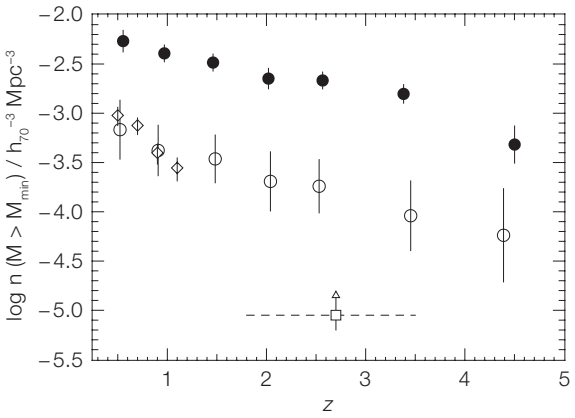

● M > 10^{10} h_{70}^{-2} $M_\odot$ (FDF + GOODS-S)
○ M > 10^{11} h_{70}^{-2} $M_\odot$ (FDF + GOODS-S)
◇ M > 10^{11} h_{70}^{-2} $M_\odot$ (MUNICS)
□ M > 10^{11} h_{70}^{-2} $M_\odot$ (Sub-mm; Tecza et al. 2004)

Figure 4: The number density of galaxies with stellar masses M > 10^{10} $M_\odot$ and M > 10^{11} $M_\odot$. Results from the MUNICS survey as well as results from Sub-mm studies are also shown.

In our lowest redshift bin, $z \sim 0.5$, the mass function follows the local mass function very well. The depth of the FDF ($I \sim 26.8$) allows us to extend the faint end of the mass function down to 10^8 $M_\odot$, a decade lower in mass than before, with no change of slope. Furthermore, the faint end slope is consistent with the local value of $\alpha \sim 1.1$ at least to $z \sim 1.5$. Our mass function also agrees very well with the MUNICS and K20 results at $z < 2$.

The mass function seems to evolve in a regular way at least up to $z \sim 2$ with the normalisation decreasing by 50 % to $z = 1$ and by 70 % to $z = 2$, with the largest change occurring at masses of M > 10^{10} $M_\odot$. These likely progenitors of today's $L > L^*$ galaxies are found in much smaller numbers above $z \sim 2$. However, we note that massive galaxies with M > 10^{11} $M_\odot$ are present even to the largest redshifts we probe (albeit in much smaller numbers). Beyond $z \sim 2$ the evolution becomes more rapid.

In Figure 4 we compare the number density evolution of massive galaxies (M > 10^{11} $M_\odot$) with that of less massive systems (M > 10^{10} $M_\odot$), combining our two survey fields. We find that high-mass galaxies evolve similarly to lower mass galaxies, and do not disappear faster with redshift.

We find that the stellar mass density at $z = 1$ is 50 % of the local value. At $z = 2$, 25 % of the local mass density is assembled, and at $z = 3$ and $z = 5$ we find that at least 15 % and 5 % of the mass in stars is in place, respectively.

The specific star-formation rate

The stellar mass content of galaxies evolves in two ways: by star formation within the galaxy, and by merging with other galaxies driven by hierarchical structure formation. Ultimately, the goal is to distinguish these two contributions to the mass build-up process. This cannot be done from measurements of the mass function alone; measurements of the star-formation rates are necessary.

We determine the star-formation rate for each galaxy in our sample from its rest-frame UV luminosity (see Gabasch et al. 2004b). Star-formation rates determined in this way suffer from problems of dust extinction. Heavily dust-enshrouded objects might escape detection completely, or, objects might be detected, but their star-formation rate (and stellar mass) might be underestimated. We try to correct for the second effect by including dust attenuation in our model fitting. However, an advantage is that in our sample, each detected galaxy has both a stellar mass and a star-formation rate measurement. In principle both of the above sources of uncertainty could be overcome with observations in the thermal infrared (albeit not without some problems of their own). Such data from the Spitzer Space Telescope are becoming available now and will be used in future papers.

In Figure 5 we show the specific star-formation rate as a function of stellar mass and age for six different redshift bins covering the range $0.4 < z < 5.0$. The upper cut-off of the specific star-formation rate runs essentially parallel to lines of constant star-formation rate and shifts to higher star-formation rates with increasing redshift. This was already noted in earlier work. This trend seems to continue to the highest redshifts probed by our sample: While at $z \sim 0.6$ we find $SFR_{max} \simeq 5$ $M_\odot$ yr^{-1}, galaxies reach as much as $SFR_{max} > 100$ $M_\odot$ yr^{-1} at $z \sim 4$. Note that this upper envelope is partly due to a selection effect: Heavily dust-obscured star bursts cannot be detected in our sample, and hence the large star-formation rates in massive galaxies at high redshift are to be regarded as lower limits. The lack of galaxies with low specific star-formation rates is due to the flux limit of the sample.

It is helpful to visualise schematically different ways to double a galaxy's mass as shown in the lower right-hand panel of Figure 5.

Quiescently star-forming galaxies: A galaxy doubling its stellar mass by quiescent star formation at 0.5 $M_\odot$ yr^{-1} moves along a line of constant star-formation rate towards the lower right part of the diagram. Note that galaxies below the doubling

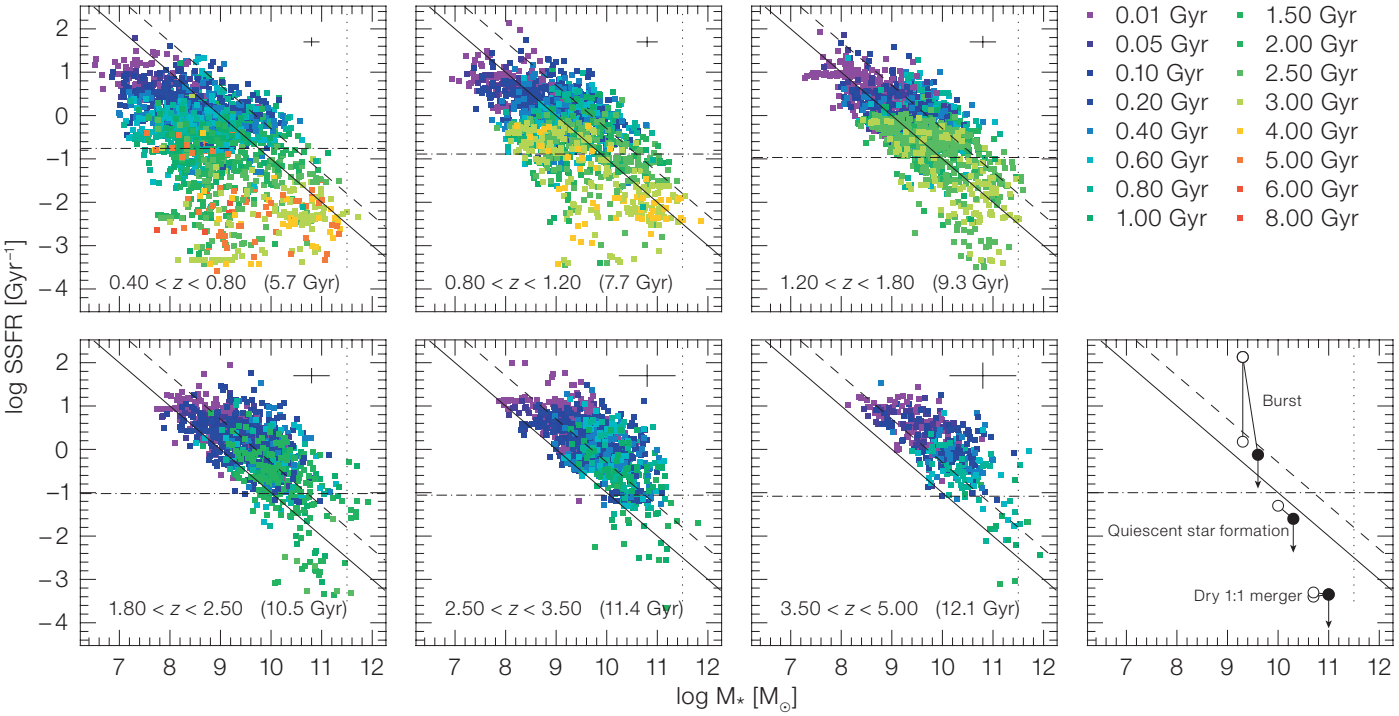

Figure 5: The specific star-formation rate as a function of stellar mass and redshift. The solid and dashed lines correspond to star-formation rates of 1 $M_\odot$ yr^{-1} and 5 $M_\odot$ yr^{-1}, respectively. Objects are coloured according to the age of their stellar population. The dot-dashed line is the specific star-formation rate required to double a galaxy's mass between each redshift epoch and today (assuming constant star-formation rate); the corresponding lookback time is indicated in each panel. **Lower right-hand panel:** Examples for evolutionary paths yielding a doubling of a galaxy's mass, through quiescent star formation, through a burst of star formation superimposed on quiescent star formation, and through a dry equal-mass merger.

line in Figure 5 do not have enough time to double their mass until the present epoch, assuming that their star-formation rate remains constant.

Starbursts: In contrast to a quiescent galaxy, a starburst can increase its mass in a shorter time interval, provided it has enough gas to consume. Bursts of star formation may be triggered by gas inflow or galaxy interactions, and quickly move a galaxy to high specific star-formation rates, where it stays for a brief period of time before it fades back. Given the typical dusty nature of starburst galaxies, they might escape detection in optical surveys during this stage, or their star-formation rates may be underestimated. However, since these bursts are typically brief, the galaxies spend most of their time with the quiescent galaxies.

Dry mergers: Two galaxies undergoing a dry merger (i.e. a merger without interaction-induced star formation) basically move to the right in the diagram. We illustrate this with equal stellar mass mergers; the stellar mass clearly doubles, while the final specific star-formation rate is the average of the two initial specific star-formation rates or below.

Note that the 'true' endpoint of the galaxies' evolution will in all three cases likely be lower than shown, since all three processes diminish the limited gas supply. This is indicated by the downward pointing arrows.

In the light of these evolutionary possibilities it is obvious that the only two ways to form massive galaxies with old stellar populations is by highly efficient early star formation in massive halos, or by dry merging of less massive galaxies harbouring old stars. Both scenarios can, in principle, be distinguished by analysing the redshift dependence of the specific star-formation rate in the most massive galaxies.

It is therefore interesting to ask when galaxies of a particular mass form most of their stars. The answer is presented in Figure 6, where we show the average specific star-formation rate as a function of redshift for galaxies in three mass intervals. At redshifts $z < 2$, the most massive galaxies with $\log M_\star/M_\odot \in [10.5, 11.5]$ are in a quiescent state with specific star-formation rates not contributing significantly to their growth in stellar mass. However, at redshifts $z > 2$, the picture changes dramatically: The specific star-formation rate for massive galaxies increases rapidly by a factor of ~ 10 until we reach their formation epoch at $z > 2$. Galaxies of lower mass seem to be forming a larger portion of their stars progressively later.

Evolution by morphology

High-resolution HST-based imaging is available in both the FDF and GOODS-S (see Figure 1). We use these images to derive quantitative morphology allowing us to discriminate between disc-dominated and bulge-dominated galaxies by their surface brightness profiles up to $z \sim 1$. In Pannella et al. 2006 we compare the evolution of the mass function of disc galaxies to that of bulge dominated galaxies. We find that the mass at which disc galaxies dominate the total mass function decreases with cosmic time, i.e., that since $z \sim 1$, mass has shifted from disc-dominated systems to bulge-dominated systems. Based on a comparison of the specific star-formation rates in disc-dominated and bulge-dominated galaxies, we conclude that merging events, and not star formation, play the key role in this process.

Figure 6: Average specific star-formation rates for galaxies with stellar masses of log $M_*/M_\odot \in$ [8.5, 9.5] (blue), [9.5, 10.5] (green) and [10.5, 11.5] (red) and star-formation rates larger than 1 $M_\odot$ yr^{-1} as a function of *z* for FDF (open squares), GOODS-S (open diamonds) and the combined sample (filled circles). The error bar represents the error of the mean. The solid line indicates the doubling line of Figure 5 which can be used to discriminate quiescent and star-forming galaxies.

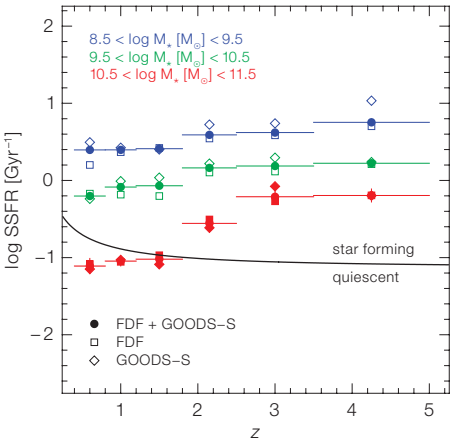

Such samples allow us to view the assembly of galaxies in principle for the first time. Also, theoretical models of galaxy formation can use these data to compare wide ranges of observables to their predictions.

Future surveys will provide yet better constraints on the current set of observables and will add further observables for each galaxy, until a complete picture of the star-formation and merging history of galaxies can be obtained.

References

Drory N. et al. 2004, ApJ 608, 742
Drory N., Bender R. and Hopp U. 2004, ApJ 616, L103
Drory N. et al. 2005, ApJ 619, L131
Feulner G. et al. 2005, ApJ 633, L9
Fontana A. et al. 2004, A&A 424, 23
Gabasch A. et al. 2004a, A&A 421, 41
Gabasch A. et al. 2004b, ApJ 616, L83
Giavalisco M. et al. 2004, ApJ 600, L93
Heidt J. et al. 2003, A&A 398, 49
Noll S. et al. 2004, A&A 418, 885
Pannella M. et al. 2006, ApJ 639, L1
Salvato M. et al. 2006, A&A, submitted

A Supernova in an Interacting Pair of Galaxies

MCG-01-39-003 (bottom right) is a peculiar spiral galaxy, apparently interacting with its neighbour, the spiral galaxy NGC 5917 (upper right). Both galaxies are located at similar distances, about 87 million light years away, towards the constellation of Libra.

Last year, a star exploded in the vicinity of the hook. The supernova, noted SN 2005cf as it was the 84th found that year, was discovered by astronomers Pugh and Li with the robotic KAIT telescope on 28 May. It appeared to be projected on top of a bridge of matter connecting MCG-01-39-003 with NGC 5917. Further analysis with the Whipple Observatory 1.5-m Telescope showed this supernova to be of the Ia type and that the material was ejected with velocities up to 15 000 km/s. Immediately after the discovery, the European Supernova Collaboration (ESC), led by Wolfgang Hillebrandt (MPA-Garching, Germany) started an extensive observing campaign on this object, using a large number of telescopes around the world. The ESC includes ten institutions across Europe (Stockholm, MPA, Barcelona, CNRS, ESO, ICSTM, ING, IoA, Padua, Oxford).

There have been several indications about the fact that galaxy encounters and/or galaxy activity phenomena may produce enhanced star formation. As a consequence, the number of supernovae in this kind of system is expected to be larger with respect to isolated galaxies. Normally, this scenario should favour mainly the explosion of young, massive stars. Nevertheless, recent studies have shown that such phenomena could increase the number of stars that eventually explode as Type Ia supernovae.

The supernova was followed by the ESC team during its whole evolution, from about ten days before the object reached its peak luminosity until more than a year after the explosion. As the SN becomes fainter and fainter, larger and larger telescopes are needed. One year after the explosion, the object is indeed about 700 times fainter than at maximum.

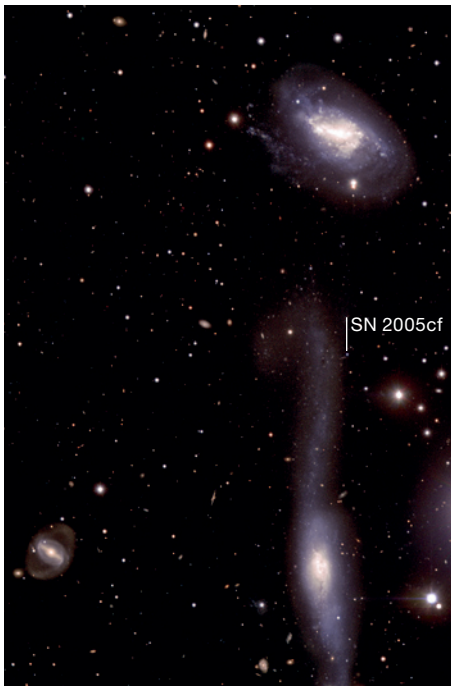

The supernova was observed with the VLT equipped with FORS1 by ESO astronomer Ferdinando Patat, who is also member of the team led by Massimo Turatto (INAF-Padua, Italy), and at a later stage by the Paranal Science Team, with the aim of studying the very late phases of the supernova. These late stages are very important to probe the inner parts of the ejected material, in order to better understand the explosion mechanism and the elements produced during the explosion. The deep FORS1 images reveal a beautiful tidal structure in the form of a hook, with a wealth of details that probably include regions of star formation triggered by the close encounter between the two galaxies.

(Based on ESO Press Photo 22/06)

ESO PR Photo 22/06 is a composite image based on data acquired with the FORS1 multi-mode instrument in April and May 2006 for the European Supernova Collaboration. The observations were made in four different filters (*B*, *V*, *R*, and *I*) that were combined to make a colour image. The field of view covers 5.6 × 8.3 arcmin. North is up and East is to the left. The observations were done by Ferdinando Patat and the Paranal Science team (ESO), and the final processing was done by Olivia Blanchemain, Henri Boffin and Hans Hermann Heyer (ESO).